# 6MAP, a Fluorescent Adenine Analogue, Is a Probe of Base Flipping by DNA Photolyase

3 **AUTHORS**, INCLUDING:

Spiridoula Matsika
Temple University
**73** PUBLICATIONS **1,440** CITATIONS

Robert J Stanley
Temple University
**47** PUBLICATIONS **962** CITATIONS

# 6MAP, a Fluorescent Adenine Analogue, Is a Probe of Base Flipping by DNA Photolyase

**Kongsheng Yang, Spiridoula Matsika, and Robert J. Stanley***

*Department of Chemistry, Temple University, Philadelphia, Pennsylvania 19122*

*Received: February 6, 2007; In Final Form: June 22, 2007*

Cyclobutylpyrimidine dimers (CPDs) are formed between adjacent pyrimidines in DNA when it absorbs ultraviolet light. CPDs can be directly repaired by DNA photolyase (PL) in the presence of visible light. How PL recognizes and binds its substrate is still not well understood. Fluorescent nucleic acid base analogues are powerful probes of DNA structure. We have used the fluorescent adenine analogue 6MAP, a pteridone, to probe the local double helical structure of the CPD substrate when bound by photolyase. Duplex melting temperatures were obtained by both UV–vis absorption and fluorescence spectroscopies to ascertain the effect of the probe and the CPD on DNA stability. Steady-state fluorescence measurements of 6MAP-containing single-stranded and doubled-stranded oligos with and without protein show that the local region around the CPD is significantly disrupted. 6MAP shows a different quenching pattern compared to 2-aminopurine, another important adenine analogue, although both probes show that the structure of the complementary strand opposing the 5′-side of the CPD lesion is more destacked than that opposing the 3′-side in substrate/protein complexes. We also show that 6MAP/CPD duplexes are substrates for PL. Vertical excitation energies and transition dipole moment directions for 6MAP were calculated using time-dependent density functional theory. Using these results, the Förster resonance energy transfer efficiency between the individual adenine analogues and the oxidized flavin cofactor was calculated to account for the observed intensity pattern. These calculations suggest that energy transfer is highly efficient for the 6MAP probe and less so for the 2Ap probe. However, no experimental evidence for this process was observed in the steady-state emission spectra.

The dynamic nature of DNA is reflected in the propensity of individual bases to pivot out of the double helix transiently in a process called base flipping.[1] More than just a curious biophysical phenomenon, these base-flipped states are important in DNA repair[2–5] and modification,[6–8] although it is not known whether the proteins responsible for these processes recognize the bases in their flipped-out states or whether they induce their substrates to flip. This is a particularly interesting question in the case of DNA photolyase (PL), a light-driven DNA repair protein that binds and repairs cyclobutylpyrimidine dimers.[9]

Photolyase is a flavoprotein that contains one flavin adenine dinucleotide (FAD) molecule as its catalytic cofactor. The protein binds cyclobutylpyrimidine dimer (CPD)-containing ss- and ds-DNA with high specificity, $K_A = 10^8$ and $10^9$ M$^{-1}$, respectively, in a light-independent step. If the FAD is in its reduced form, the absorption of a blue photon will result in highly efficient repair of the CPD in about 3 ns.[9] This process is under study in several laboratories.[10–15] Crystal[16,17] and NMR[18] structures of the protein and protein:substrate complex show that the CPD is flipped out of the double helix into a cavity in the protein in close proximity to the FAD cofactor. The details of this binding mechanism have been studied by a variety of biochemical and biophysical approaches.[5,19,20] It is not known whether the CPD is flipped out by the action of the protein, or whether spontaneous flipping of the CPD yields a transient species that is recognized by the protein and is subsequently bound for repair. Serendipitously, oxidized photolyase (PL$_{ox}$) will bind but *not* repair CPDs,[21] making the

oxidized protein:substrate complex an excellent system for studying substrate binding.

We have shown in previous work that 2-aminopurine (2Ap), a fluorescent adenosine analogue (see Scheme 1), is an excellent probe of base flipping in PL.[5] 2Ap has an excitation maximum around 306 nm with an emission maximum around 370 nm.[22] The fluorescence quantum yield of 2Ap has been shown to be sensitive to base stacking.[23] Our results[19] show that this fluorescent analogue can reliably report on the differential distortion experienced by the complementary strand of the substrate DNA upon binding to the protein, as corroborated by the crystal structure.[17]

6MAP (4-amino-6-methyl-8-(2′-deoxy-$\beta$-D-ribofuranosyl)-7(8$H$)-pteridone; see Scheme 1) is a relatively new fluorescent adenosine analogue.[24,25] DNA containing 6MAP shows steady-state fluorescence excitation and emission spectra with maxima at 330 and 430 nm, respectively.[24] The monomer has a high fluorescence quantum yield ($\Phi_f \sim 0.4$). When incorporated into single- and double-stranded DNA, $\Phi_f$ decreases due to base stacking, indicating that the molecule can report on local structural changes in these systems. The mechanism of this fluorescence quenching is not understood at present. Unlike 2-aminopurine, 6MAP quenching does not depend obviously on the chemical identity of its nearest neighbors.

A very attractive feature of 6MAP as an internal probe of DNA structure compared to 2Ap is that both its absorption and emission spectra are comparatively red-shifted. Fortuitously, the emission spectrum of 6MAP, with a Stokes shift of about 100 nm, overlaps the $S_0 \rightarrow S_1$ absorption transition of oxidized FAD (FAD$_{ox}$) very closely. This makes Förster resonance energy transfer (FRET) a possibility when the 6MAP is excited. If so, then this probe would provide an excellent tool to study the

* Corresponding author: Telephone: (215) 204-2027. E-mail: rstanley@temple.edu.

**SCHEME 1**



2Ap                          Thymine



6MAP                          Thymine
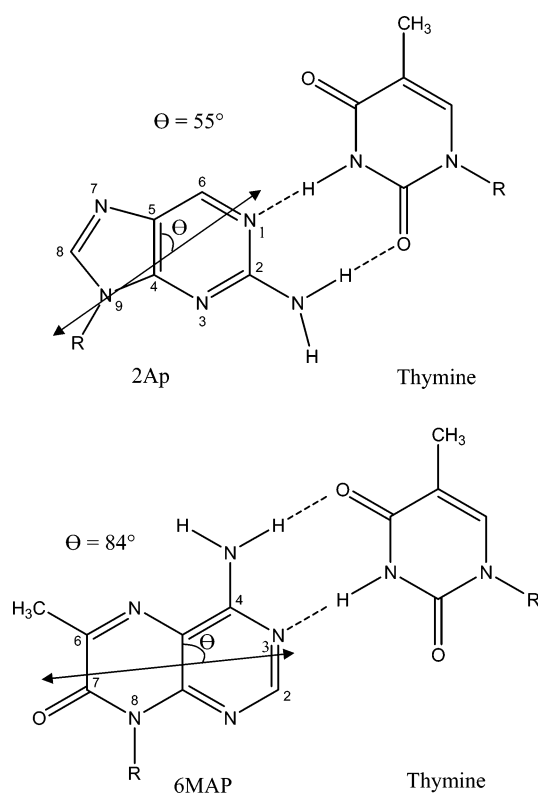
dynamics of the photolyase:substrate complex as well as its structure. FRET should also be possible with 2Ap-containing DNA because its emission overlaps the $S_0 \rightarrow S_2$ absorption band of $FAD_{ox}$. Internal conversion between $S_2$ and $S_1$ occurs efficiently on the picosecond time scale,[26] which in turn results in flavin emission from the $S_1$ state.

In this study, we show that 6MAP is a sensitive probe of CPD base flipping by photolyase and that the probe does not interfere with the repair of the substrate. Absorption spectra of ss- and ds-DNA were obtained. The thermostability of double helices containing 6MAP and a CPD were estimated from thermal melting profiles. The emission spectra of 6MAP-labeled DNA in the presence and absence of PL are shown, and the intensity patterns and emission maxima are discussed. We also present the results of TDDFT calculations to estimate the direction of the transition dipole moment for the lowest excited-state transition of 6MAP and use this result to calculate FRET efficiencies for 6MAP-containing duplexes complexed with the protein. These are compared with FRET efficiencies calculated for the corresponding 2Ap-containing complexes.

**Experimental Procedures**

**Photolyase Protein.** *Escherichia coli* DNA photolyase was overexpressed in JM109 cells transformed with the pMS969 plasmid containing the *phr* gene (the plasmid was a generous gift of Professor Aziz Sancar, University of North Carolina, Chapel Hill, NC). The purification of the protein was based on the method of Payne et al.[27] and modified as described in detail in a previous paper.[28] Apoprotein and PL reconstituted with $FAD_{ox}$ (rPL) were prepared as described in ref 19. The purity of rPL was determined by the ratio of absorbances at $\lambda = 280$ nm (protein) and 450 nm (FAD). The ratio of $A_{280}/A_{450}$ was typically around 16. Pure protein would have a ratio of about 12, based on the known extinction coefficients of the apoprotein and FAD-reconstituted protein.[29] This indicates that protein

purity was about 75%. Further purification was deemed unnecessary as apophotolyase does not bind substrate.[30]

**DNA Oligonucleotides: Irradiation and Purification.** The oligonucleotides used in this study were as follows:

T-T:   5′-GCAAGTTGGAG-3′

CPD or T<>T:   5′-GCAAGT<>TGGAG-3′

A-A:   5′-CTCCAACTTGC-3′

3′-6MAP:   5′-CTCCA$\underline{P}$CTTGC-3′

5′-6MAP:   5′-CTCC$\underline{P}$ACTTGC-3′

where T-T stands for the complementary strand, T<>T indicates the complementary strand containing a cyclobutylpyrimidine dimer, and the underlined $\underline{P}$ indicates the position of the fluorescent base analogue in the 6MAP-containing ss-DNA. Double reverse phase (RP)-HPLC purified 6MAP-containing oligonucleotides were purchased from TriLink Biotechnologies. The other double RP-HPLC purified 11-mer oligonucleotides include the complementary sequence (T-T) and a control sequence (A-A) which were purchased from Integrated DNA Technologies, Inc. In addition, 2Ap-containing ss-DNA having the same sequence as the 3′-6MAP and 5′-6MAP oligos (named 3′-2Ap and 5′-2Ap, respectively) were also purchased from the same company. All oligonucleotides were resuspended in HPLC-grade water and used without further purification except T<>T, which was processed as given below.

Some T-T oligonucleotide was irradiated with UV-B light to produce the CPD-containing complementary oligonucleotide, T<>T.[31] Irradiation of a solution of $8.4 \times 10^{-2}$ mM T-T 11-mer and $1-2$ mM acetophenone was performed in a 1 mm quartz cuvette sealed with a septum. The cuvette was first purged with argon for 30 min to remove oxygen and placed on ice. The cell was covered with a plastic Petri dish to filter out wavelengths below ~310 nm and irradiated for 4 h using two Phillips Ultraviolet-B 40 W bulbs at a distance of about 10 cm. Following irradiation, the solvent was removed using a Savant Speed Vac SC110. The pellet was then resuspended in 100 $\mu$L of HPLC-grade water.

The T<>T oligonucleotide was purified using a Rainin HPLC with a Waters 8 × 100 mm radial compression Nova-Pak $C_{18}$ column. A linear gradient of 7.0−9.0% acetonitrile was used against 100 mM tetraethylammonium acetate over 20 min at 1 mL/min with detection at 260 nm.[31] The T<>T oligonucleotide was collected and desiccated to dryness, resuspended in HPLC-grade water, and loaded onto a YMC 4.6 × 250 mm ODS-AQ HPLC $C_{18}$ column. After running 10 min at 100% HPLC water, the desalted T<>T oligonucleotide was eluted with 1:1 acetonitrile/water over 10 min at 1 mL/min with detection at 260 nm. It was stored at −20 °C following desiccation until used.

**Monomer Analogue.** 6MAP nucleoside, a kind gift from Mary Hawkins (NIH), was dissolved in ethanol and kept at −20 °C until needed. Samples for analysis were made by diluting 6MAP stock with buffer T (50 mM phosphate, 100 mM potassium chloride, 0.1 mM EDTA, and 10 mM $\beta$-mercaptoethanol, pH 7.5). Monomer 2-aminopurine was obtained from ACROS and used without further purification. Fresh solutions were made by diluting a 16 $\mu$M stock solution of 2Ap in the appropriate solvent to the indicated concentration.

**Melting Temperature Measurements.** Both fluorescence emission and UV−vis absorbance methods were used to determine the melting point of the duplexes. For the fluorescence

6MAP, a Probe of Base Flipping by DNA Photolyase

*J. Phys. Chem. B, Vol. 111, No. 35, 2007* **10617**

emission measurements, samples were prepared fresh for each scan. Different mixtures of oligonucleotides were placed in sterile Eppendorf tubes in minimal volume, typically less than 50 $\mu$L. These samples were heated in a 75−80 °C water bath for 10 min and allowed to cool to room temperature on the laboratory bench for at least 30 min. Samples for study were diluted to 1 mL with buffer T.

A constant wavelength analysis as a function of temperature was performed with excitation at 330 nm and emission at 430 nm with 5 nm slits using a SPEX Fluoromax-2. The fluorimeter cuvette holder was connected to a temperature-variable circulating water bath set to 10 °C. To obtain a melting curve, the temperature on the controller was set to 85 °C, giving a ramp of about 2 °C/min, and spectra were recorded at 15 s intervals. Each melting curve was repeated in triplicate.

A calibration of the temperature ramp was achieved inside the cuvette by measuring the temperature at 15 s intervals using a thermocouple (OMEGA K type HH22). Three replicants were averaged and fitted to a fifth-order polynomial to obtain the temperature profile as a function of time. The difference between the fifth-order fit and the calibration curve were sufficiently small that a higher order fit was deemed unnecessary.

For the absorbance method, samples were prepared as described above. Absorbance spectra were obtained using a Hewlett-Packard HP8452A diode-array spectrophotometer. Absorbance spectra as a function of temperature were measured using the time-based kinetics mode of the spectrometer. Data were taken from 240 to 420 nm with an integration time of 2 s and a resolution of 2 nm. The temperature axis was calibrated as described above. The average absorbance from 240 to 280 nm was baseline-corrected by subtracting the average absorbance from 400 to 420 nm. A 1.0 cm path length, 0.10 cm wide black-walled quartz cell was used. The cuvette was allowed to equilibrate in the holder for 10 min prior to a scan. A similar scan was obtained for the buffer, and its baseline-corrected temperature-dependent absorbance was used to correct that of the sample absorbance determined as described above.

**Thermodynamic Parameters.** The melting point of a DNA duplex, $T_m$, is defined as the temperature at which half of the duplexes have dissociated, or when [probe·complementary] = [probe]. The dissociation constant, $K_d$, is based on the equilibrium equation

$$K_d = \frac{[\text{probe}][\text{comp}]}{[\text{probe·comp}]} \quad (1)$$

where the bracketed quantities refer to the equilibrium concentrations of the double- and single-stranded DNA. This dissociation constant is temperature dependent. Thermodynamic parameters were obtained by an analysis of the temperature-dependent melting of the duplexes. The extinction coefficients of both single- and double-stranded DNA were presumed to depend linearly on the temperature,[32−34] with the assumption that the slope for both probe and complementary strands was the same:

$$\epsilon_{ds} = m_{ds}T + b_{ds} \quad (2a)$$

$$\epsilon_p = m_p T + b_p \quad (2b)$$

$$\epsilon_c = m_c T + b_c \quad (2c)$$

where $\epsilon_{ds}$, $\epsilon_p$, and $\epsilon_c$ are the extinction coefficients for the double-stranded DNA, single-stranded probe, and single-stranded complementary DNA, respectively. The slopes ($m$) and

intercepts ($b$) are defined for each species. Here the assumption has been made that the probe strand has an extinction of approximately $0.82\epsilon_c$ at $T = 0$ K, based on the calculated extinction coefficients. The change in absorption as a function of temperature is

$$\Delta A(T) = [\text{ds}]\epsilon_{ds}(T) + [\text{probe}]\epsilon_p(T) + [\text{comp}]\epsilon_c(T) \quad (3)$$

These concentrations were calculated according to eq 4:

$$K_d(T) = \exp\left(-\frac{\Delta H°}{RT} + \frac{\Delta S°}{R}\right) \quad (4)$$

where the equilibrium concentrations of the ds- and ss-DNA from eq 1 were determined by a nonlinear-least-squares minimization (lsqcurvefit, MATLAB, The Mathworks), giving the best fit parameters $\Delta H°$, $\Delta S°$, $\epsilon_{ds}$, $\epsilon_p$, $b_{ds}$, $b_p$, and $b_c$. The change in the Gibbs free energy was calculated at 37 °C using $\Delta G_{37}° = \Delta H° - (310.2 \text{ K})\Delta S°$.

The optimized parameter set was then randomized to generate initial values to test the sensitivity of the fit to the parameters.[35] The standard deviations of the parameters generated by this procedure are reported along with the parameters (see below).

**Repair Assay.** Substrate repair was monitored by measuring the change in 6MAP fluorescence of a 6MAP/CPD duplex in the presence of reduced PL. Photolyase was reduced using sodium dithionite by first deoxygenating a 400 nM solution of protein in buffer T in a fluorescence cuvette and then adding 4−10 equiv of a stock solution of dithionite, made fresh in the same buffer. The cuvette was sealed with a rubber septum and the solution was incubated for 1 h on ice to allow excess dithionite to form bisulfite. The target duplex, containing the substrate strand and a complementary strand with either a 5′- or 3′-6MAP probe, was added anerobically under a nitrogen atmosphere in a glovebag.

The cuvette was placed in the fluorimeter and subjected to photoreactivating 365 nm radiation from the fluorometer 150 W Xe arc lamp through a 30 nm band-pass slit for various amounts of time. The fluorimeter was then used to record the fluorescence intensity of the 6MAP fluorophore with excitation at 330 nm (8 nm band pass) and emission at 430 nm (4 nm band pass).

**Steady-State Fluorescence Emission Spectra.** Fluorescence samples were prepared in the same fashion as described for the melting point experiments (see above). If appropriate, PL$_{ox}$ was added and the samples were then brought to a total volume of 1 mL in buffer T. The fluorescence cuvette containing the sample was sonicated briefly in a small ultrasonic bath to remove bubbles before each measurement.

The fluorescence from 6MAP-containing samples was scanned from 350 to 575 nm with excitation at 330 nm. The scans were taken with an integration time of 0.2 s, a step size of 2 nm, and an excitation band pass and emission band pass of 8 and 4 nm, respectively. The emission intensity was ratioed to the excitation intensity to remove fluctuations from Xe lamp drift and to normalize the emission spectra to the excitation fluence. Three replicates of each emission spectrum were averaged together. The excitation and emission light were unpolarized. Spectra were corrected for the background fluorescence and Raman scattering of the buffer or control sample and corrected for the wavelength bias of the fluorimeter. A photobleaching control was performed using the 3′-6MAP/CPD duplex under the illumination conditions used for the emission spectra. Less than 6% decrease in the 6MAP emission was obtained, indicating that photobleaching of the analogue is small. In addition, the fluorescence spectra were corrected for differences in the absorption of the samples

due to electronic effects (see below). A 0.40 × 1.0 cm fluorescence quartz cell was used as described above. All measurements were made at 15.0 ± 0.1 °C.

**Förster Resonance Energy Transfer Calculations.** The efficiency of energy transfer, $\phi_{ET}$, is related to the distance ($r_{DA}$) between the donor (adenine analogue) and the acceptor (FAD in photolyase) by

$$\phi_{ET} = \frac{R_0^6}{R_0^6 + r_{DA}^6} \quad (5)$$

$R_0$ is the Förster distance where the efficiency of energy transfer is 50%. The value of $R_0$ can be calculated from

$$R_0 \,(\text{Å}) = 0.211(\kappa^2 n^{-4} \phi_D J)^{1/6} \quad (6)$$

where $\kappa^2$ is the orientation factor, $n$ is the refractive index of the medium (assume $n = 1.33$ for aqueous solutions), $\phi_D$ is the fluorescence quantum yield of the donor, and $J$ is the overlap integral. The orientation factor is essentially the angular relationship between the transition dipole moments of the donor and acceptor:

$$\kappa^2 = (\cos\theta_T - 3\cos\theta_D \cos\theta_A)^2 \quad (7)$$

where $\theta_T$ is the angle between the emission dipole of the donor and the absorption dipole of the acceptor, and $\theta_D$ and $\theta_A$ are the angles between these dipoles and the vector joining the donor and the acceptor, respectively. Swiss-PdbViewer (version 3.7) was used to estimate the distances and angles between atoms and molecules in the photolyase:DNA complex. The overlap integral ($J$) between adenine analogues and oxidized FAD in photolyase can be obtained from

$$J = \frac{\int F_D(\lambda)\, \epsilon_A(\lambda) \lambda^4 \, d\lambda}{\int F_D(\lambda)\, d\lambda} \quad (8)$$

where $\lambda$ is the wavelength of the light in nanometers, $\epsilon_A(\lambda)$ is the molar extinction coefficient of the acceptor at that wavelength, and $F_D(\lambda)$ is the fluorescence intensity of the donor as a function of wavelength.

**Computational Methods.** The excited states of 6MAP were investigated using density functional theory (DFT) employing the B3LYP functional.[36] The standard Gaussian 6-31G* basis set was used for all atoms.[37] The equilibrium geometry of the ground state was obtained using DFT. Vertical excitation energies and transition dipole moments were then calculated using time-dependent DFT (TDDFT). All calculations were carried out using the NWChem computational package.[38]

## Results

**Absorption Spectra of ss- and ds-DNA with 6MAP.** Absorption spectra of both ss- and ds-DNA oligos containing the 6MAP probe in buffer T without $\beta$-mercaptoethanol are shown in Figure 1. The 6MAP strand concentration was kept at 1.79 $\mu$M in all cases, but the concentrations of T-T and CPD strands in the duplexes were 2.50 and 3.57 $\mu$M, respectively. These concentrations were arrived at based on the results of titration experiments (see below) that showed that the degree of fluorescence quenching depended on complementary strand concentration. Enough complementary DNA was used to ensure that the fluorescence quenching reached a steady-state value for the given 6MAP probe concentration.
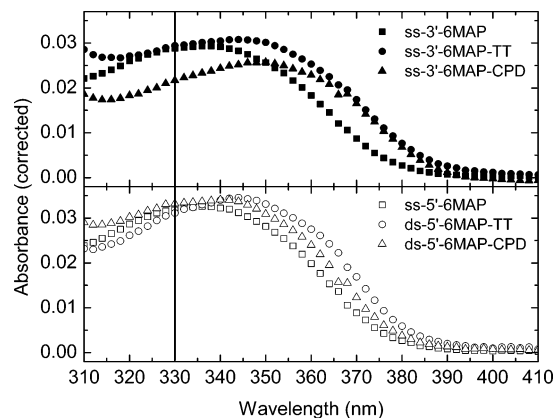


**Figure 1.** Absorption spectra of ss- and ds-DNA 6MAP-containing oligos. The closed symbols indicate the 3′-6MAP probe (top panel), and the open symbols indicate the 5′-6MAP probe (bottom panel). The 6MAP concentration was 1.79 $\mu$M for all spectra. Square symbols (□ or ■) are the ss-6MAP oligos, circles (○ or ●) are the 6MAP oligo annealed to the undamaged complementary strand (2.50 $\mu$M), and triangles (△ or ▲) indicate duplexes of the 6MAP oligo with a CPD-containing complementary strand (3.57 $\mu$M). The line at 330 nm is given to indicate the excitation used in subsequent fluorescence measurements.

**TABLE 1: Absorption Maxima and Spectral Shifts (6-MAP Concentration = 1.8 $\mu$M)**

| DNA | $A$ (OD) | $\lambda_{max}$ (nm) | $E$ (cm$^{-1}$) | shift[a] (cm$^{-1}$) |
|---|---|---|---|---|
| ss-3′-6MAP | 0.029 | 338 | 29 586 | N/A |
| ds-3′-6MAP/T-T | 0.022 | 350 | 28 571 | 1015 |
| ds-3′-6MAP/T<>T | 0.029 | 340 | 29 070 | 516 |
| ss-5′-6MAP | 0.032 | 336 | 29 762 | N/A |
| ds-5′-6MAP/T-T | 0.031 | 344 | 29 070 | 692 |
| ds-5′-6MAP/T<>T | 0.033 | 340 | 29 412 | 350 |

[a] $E_{ss} - E_{ds}$.

The absorbances and absorption maxima are tabulated in Table 1. The most interesting result is the significantly lower absorbance of the 3′-6MAP/T-T duplex compared with the others. This duplex also showed the longest wavelength absorption maximum at 350 nm, more than 6 nm longer than the corresponding 5′-6MAP/T-T duplex. The absorption at 330 nm of 0.022 is about 30% lower relative to an average absorption of 0.031 ± 0.002 calculated for the other oligos.

Hypochromicity values[39] for the duplexes were calculated using absorption spectra of the ss-6MAP, ss-T-T, and ss-T<>T oligos (data not shown). The 3′-6MAP/T-T shows a significantly larger hypochromicity than all other cases. This may be attributable to the orientation of the 6MAP transition dipole moment to its neighbors (3′: A$\underline{P}$C vs 5′: C$\underline{P}$A) and remains an open question. However, the differences in absorption have been taken into account when correcting the fluorescence emission intensities shown below.

Table 1 also tabulates the spectral shifts of the ds-DNA oligos relative to their ss-6MAP probe strands. As a point of reference, the absorption maximum of the monomer 6MAP nucleoside in methanol is 329 nm (30 395 cm$^{-1}$).[24] The ss-5′-6MAP absorption maximum was at a slightly higher energy than the ss-3′-6MAP oligo, a difference of 176 cm$^{-1}$. This ordering was obtained in the duplexes as well. A blue shift as a result of annealing was largest for the 3′-6MAP system. The 3′-6MAP/T-T duplex gave a shift of 1015 cm$^{-1}$ compared to a 692 cm$^{-1}$ shift for the 5′-6MAP/T-T duplex. The fact that these duplexes return a blue shift is attributable to a more hydrophobic environment for the probe in duplex DNA compared to the more

6MAP, a Probe of Base Flipping by DNA Photolyase

*J. Phys. Chem. B, Vol. 111, No. 35, 2007* **10619**

solvent exposed structure in the single-stranded state. This is also consistent with the fluorescence intensities and fluorescence maxima measured, as described below.

The 3′-6MAP/T<>T oligo gave a shift of 516 cm$^{-1}$ compared to a 350 cm$^{-1}$ shift for the 5′-6MAP/T<>T duplex. These shifts are smaller than their T-T counterparts, suggesting that the CPD introduces a structural perturbation that results in a more solvent exposed probe. The observation that the 3′-duplex shows a larger blue shift than the 5′-duplex is surprising, since it is at odds with the crystal structure of a decamer DNA duplex obtained by Taylor's group. They showed that the inclusion of a CPD disrupts base stacking on the 3′-side of the complementary A-A tract more than on the 5′-side.[40] This should lead to a smaller blue shift than for the 5′-side. However, as indicated above, there may be other electronic effects at play, which would not be evident without a more extensive exploration of how sequence modulates the electronic structure of the 6MAP probe.

Although the absolute value of the shifts are different for the T-T vs T<>T duplexes, the fractional change for the 5′ and 3′ T<>T duplexes relative to the 6MAP/T-T shift is the same, suggesting that the 6MAP probe sees the same change in solvent exposure in going from an undamaged complementary strand to a CPD-containing strand.

**Melting Temperatures of Probe- and CPD-Containing Duplexes.** We performed titration experiments to determine the ratio of probe concentration to either T-T or CPD strand concentrations at which all probe strands form double helical DNA with the opposing strand. This control was performed using fluorescence detection to determine the ratio of complement to probe oligo necessary to achieve maximal quenching (data not shown). Based on these experiments, the T<>T and T-T oligos were used in ratios of 2.0 and 1.4, respectively, relative to the probe-containing strand for both 5′- and 3′-6MAP probes. This ratio of complement strand to probe strand was maintained in all subsequent experiments.

We focus first on the absorbance melting point experiments. The temperature dependence of the absorbance reflects changes in hypochromism due to the stacking of bases in the duplex. As discussed above, the change in absorption as a function of temperature was modeled assuming that the extinction of the duplex and single strands vary linearly with temperature, and that the equilibrium concentrations are temperature dependent. The fitted absorption melting curves for the A-A/T-T (control) duplex, the A-A/T<>T duplex, the 5′-6MAP/T-T and 5′-6MAP/T<>T duplexes, and the 3′-6MAP/T-T and 3′-6MAP/T<>T duplexes are shown in Figure 2. Open circles and filled squares represent the data for the CPD and T-T scans, respectively, and the solid lines indicate the fit as described above. Each data set is an average of three individual runs. It should be pointed out that while the concentration of the 6MAP strand was constant for all absorbance melting curves, the concentrations of the T<>T- or T-T-containing oligos were different, based on the results of the titration experiments above. Specifically, the concentration of the CPD-containing oligo was higher than that of the T-T-containing oligo for the same concentration of probe strand. However, the duplex concentrations were the same. In addition, the extinction coefficient of the T<>T oligo at 260 nm is about 9/11 that of the T-T 11mer. Therefore, the change of absorbance during the melting for CPD-containing duplex was smaller than that of T-T-containing duplex.

The fitting parameters $\Delta H°$, $\Delta S°$, and the calculated $T_m$ and $\Delta G_{37}°$ are given in Table 2. Comparison with the control duplex (A-A/T-T) suggests that the introduction of a CPD lowers the
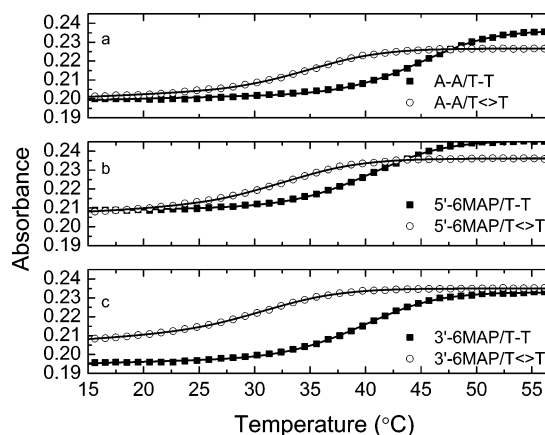


**Figure 2.** DNA melting curves determined by UV−vis absorption for CPD-containing duplexes (■, 500 nM in 6MAP oligo and 900 nM in CPD), and undamaged duplexes (○, 500 nM in 6MAP oligo and 700 nM in T-T). The solid lines are fits based on a two-state model. Panel a shows the A-A/T-T (control, 500 nM in A-A oligo and 700 nM in T-T, ■) and A-A/T<>T duplexes (500 nM in A-A oligo and 900 nM in CPD, ○). Panel b shows the 5′-6MAP-containing duplexes, and panel c shows the 3′-6MAP-containing duplexes (same symbol scheme as for the control). Salt concentration was about 110 mM.
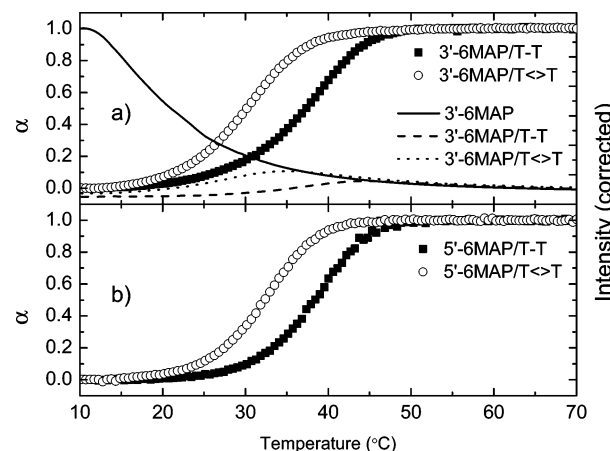


**Figure 3.** (a) DNA melting curves for the 3′-6MAP system obtained by measuring fluorescence intensity versus temperature. Collisional quenching is seen at higher temperatures for the ss-3′-6MAP (−, 250 nM), and 3′-6MAP/T-T (− −, 250 nM/350 nM) and 3′-6MAP/T<>T (---, 250 nM/600 nM) duplexes. The data have been converted to fractional dissociation, α, as described in the text. The corrected dissociation curve for 3′-6MAP/T-T is indicated by ■ and the 3′-6MAP/T<>T by ○. (b) Normalized fluorescence melting curves for the 5′-6MAP duplexes (concentrations as given for the 3′ system). The corrected dissociation curve for 5′-6MAP/T-T is indicated by ■ and the 5′-6MAP/T<>T by ○). Salt concentration was about 150 mM.

**TABLE 2: Thermodynamic Parameters for DNA Duplexes from Absorbance Melting Curves**

| duplex | $T_m$ (°C) | $\Delta H°$ (kcal/mol) | $\Delta S°$ (kcal mol$^{-1}$ K$^{-1}$) | $\Delta G_{37}°$ (kcal/mol) |
|---|---|---|---|---|
| A-A/T-T | 45.2 | −79.4 (1.6) | −0.220 (5) | −11.0 |
| A-A/T<>T | 35.5 | −68.6 (1.7) | −0.194 (5) | −8.5 |
| 5′-6MAP/T-T | 40.7 | −74.2 (1.2) | −0.207 (4) | −9.9 |
| 5′-6MAP/T<>T | 33.4 | −63.7 (1.3) | −0.179 (4) | −8.0 |
| 3′-6MAP/T-T | 40.1 | −73.9 (1.2) | −0.207 (4) | −9.7 |
| 3′-6MAP/T<>T | 31.7 | −63.0 (0.8) | −0.178 (3) | −7.7 |

melting point by about 10 °C. Correspondingly, $\Delta H°$ values are about 11 kcal/mol less stable for the CPD-containing duplex compared to the control. The change in entropy suggests that the CPD-containing duplex is already somewhat disordered, and this is corroborated by the fluorescence measurements shown below. The free energy for the A-A based duplexes shows that

the introduction of a CPD creates a loss of 2.5 kcal/mol relative to the perfectly annealed duplex.

Interestingly, the introduction of 6MAP leads to a melting point depression of about 4−5 °C for either the 5′ or 3′ position in the presence of the T-T strand. $\Delta\Delta H°$ values ($=\Delta H°_{\text{control duplex}} - \Delta H°_{\text{6MAP duplex}}$) for the probe/T-T duplexes are also very similar, and both values are depressed by about −5.2 and −5.5 kcal/mol compared to the A-A/T-T control. The effect of 6MAP position on $\Delta\Delta S°$ ($=\Delta S°_{\text{control duplex}} - \Delta S°_{\text{6MAP duplex}}$) is small, with $\Delta\Delta S° \sim -0.013$ kcal mol$^{-1}$ K$^{-1}$ for the control vs 5′-6MAP or 3′-6MAP duplexes. The calculated free energy is still largest for the control duplex (−11 kcal/mol) and drops modestly for the 5′- and 3′-probe/T-T duplexes (−9.9 and −9.7 kcal/mol, respectively). Taken together, the data suggest that 6MAP in the 5′ position is slightly more stable than 6MAP in the 3′ position. A further discussion of these differences is given below.

The incorporation of a CPD opposing the probe led to a lower melting point compared with the A-A/T<>T control duplex. For the 5′-6MAP/T<>T, $\Delta T_m \sim -2$ °C, but for 3′-6MAP/T<>T, $\Delta T_m \sim -4$ °C compared to A-A/T<>T. The enthalpy changes track changes in the melting points: $\Delta\Delta H° \sim -5$ kcal/mol for A-A/T<>T → 5′-6MAP/T<>T and $\Delta\Delta H° \sim -5.6$ kcal/mol for A-A/T<>T → 3′-6MAP/T<>T. Entropy changes follow the same trend: $\Delta\Delta S° \sim -0.015$ kcal mol$^{-1}$ K$^{-1}$ and $\Delta\Delta S° \sim -0.016$ kcal mol$^{-1}$ K$^{-1}$. The corresponding changes in the free energies are $\Delta\Delta G_{37}° = -0.5$ kcal/mol and $\Delta\Delta G_{37}° = -0.8$ kcal/mol, respectively.

The fluorescence-detected melting curves are shown in Figure 3. The top panel shows in detail how each signal associated with the 3′-6MAP probe changes with temperature. The solid curve in panel a shows the change in fluorescence intensity (right axis) of the 3′-6MAP single-stranded molecule. The loss of fluorescence with increasing temperature is clearly nonlinear, having an approximately exponential decay. This decay is presumably due to collisional quenching of the excited 6MAP base by solvent[41] as any residual base stacking is lost at higher temperature. The dashed and dotted lines are the temperature-dependent fluorescence signals from 3′-6MAP/T-T and 3′-6MAP/T<>T, respectively. The fluorescence of these duplexes increased as the temperature approached $T_m$. After melting, the fluorescence intensity decreased and eventually matched the ss-3′-6MAP signal as the 6MAP probe is exposed to solvent.

It was deemed inappropriate to apply the same two-state analysis to the fluorescence-detected melting curves as was done for the absorbance curves. In the latter case, the extinction of the oligos was assumed to be linear with temperature. The nonlinear temperature dependence of the fluorescence decay of the single-strand probe complicates this approach. In addition, others have observed premelting transitions in 6MAP-containing duplexes that suggest a two-state model is insufficient.[42] However, an approximate melting point was estimated by converting the intensity curves to degree of dissociation, $\alpha$, where $T_m = T(\alpha=0.5)$. The dissociation curves for duplexes containing the 3′-6MAP probe are shown in panel a (left axis). $T_m$ values for 3′-6MAP/T-T (■) and 3′-6MAP/T<>T (○) were 37.4 and 30.2 °C, respectively. Panel b shows the 5′-6MAP/T-T (■) and 5′-6MAP/T<>T (○) data, which gave melting points of 38.5 and 32.4 °C, respectively. The melting points determined by fluorescence were ∼2−3 °C lower than those derived from the absorbance curves for the T-T duplexes and about 1 °C lower than those containing the CPD.

**Emission Spectra for 6MAP-Containing Oligomers.** The emission spectra of 6MAP-containing ss-DNA, ds-DNA, and
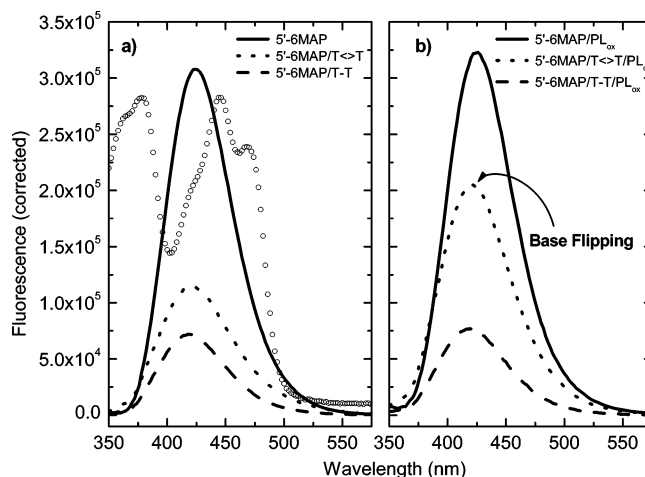


**Figure 4.** Fluorescence spectra of 5′-6MAP containing oligos at 15 °C. (a) Single-stranded 5′-6MAP 11-mer (—, 250 nM), 5′-6MAP/T-T duplex (− −, 250 nM/500 nM), and 5′-6MAP/T<>T duplex (---, 250 nM/500 nM). The open circles (○) show the (scaled) absorption spectrum of PL$_{ox}$ for comparison. (b) 5′-6MAP/PL$_{ox}$ (—, 250 nM/570 nM), 5′-6MAP/T-T/PL$_{ox}$ (− −, 250 nM/500 nM/570 nM), and 5′-6MAP/T<>T/PL$_{ox}$ (---, 250 nM/500 nM/570 nM). Salt concentration was about 150 mM.
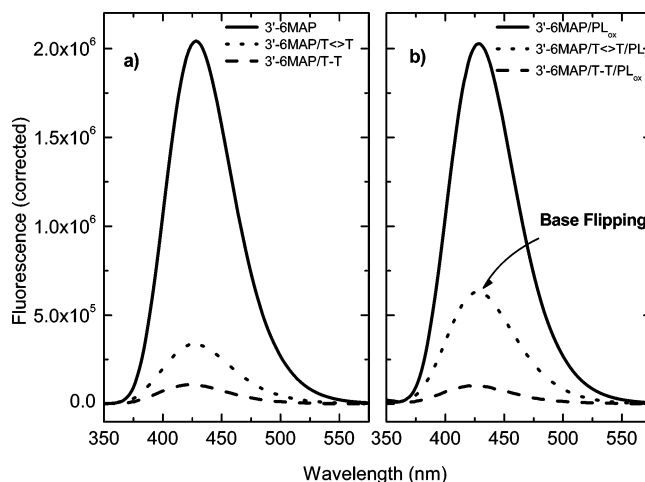


**Figure 5.** Fluorescence spectra of 3′-6MAP containing oligos at 15 °C. (a) Single-stranded 3′-6MAP 11-mer (—), 3′-6MAP/T-T duplex (− −), and 3′-6MAP/T<>T duplex (---). (b) 3′-6MAP/PL$_{ox}$ (—), 3′-6MAP/T-T/PL$_{ox}$ (− −), and 3′-6MAP/T<>T/PL$_{ox}$ (---). Salt concentration was about 150 mM. Concentrations of oligos and protein are as given for the 5′ system.

ss-DNA and ds-DNA with oxidized photolyase were measured with excitation at 330 nm. Figure 4a shows spectra of buffered DNA samples without protein, consisting of 0.25 $\mu$M 5′-6MAP oligonucleotide (—, 5′-6MAP), 0.25 $\mu$M 5′-6MAP oligonucleotide annealed to 0.35 $\mu$M T-T oligo (− −, 5′-6MAP/T-T), and 0.25 $\mu$M 5′-6MAP oligonucleotide annealed to 0.50 $\mu$M T<>T oligonucleotide (---, 5′-6MAP/T<>T). Emission spectra for 5′-6MAP-containing DNA with photolyase—0.25 $\mu$M 5′-6MAP/0.57 $\mu$M PL$_{ox}$ (—, 5′-6MAP/PL$_{ox}$), 0.25 $\mu$M 5′-6MAP/0.35 $\mu$M T-T/0.57 $\mu$M PL$_{ox}$ (− −, 5′-6MAP/T-T/PL$_{ox}$), and 0.25 $\mu$M 5′-6MAP/0.50 $\mu$M T<>T/0.57 $\mu$M PL$_{ox}$(---, 5′-6MAP/T<>T/PL$_{ox}$)—are given in Figure 4b. Also shown is the absorption spectrum of PL$_{ox}$ (○, scaled for comparison). Figure 5 presents emission spectra using the 3′-6MAP oligo under the same conditions as described for the 5′-6MAP spectra. A control sample of 0.57 $\mu$M PL$_{ox}$ was also scanned and subtracted from the spectra to remove buffer and protein fluorescence and Raman scattering (scan not shown). Each spectrum is the average of at

6MAP, a Probe of Base Flipping by DNA Photolyase

*J. Phys. Chem. B, Vol. 111, No. 35, 2007* **10621**

**TABLE 3: Integrated Fluorescence Emission from 350 to 575 nm of 6MAP (Probe) Containing Oligonucleotides with and without $PL_{ox}$**

| sample | 3′-6MAP* $\lambda_{max}$ | $\int I_{3'-6MAP*}$ d$\lambda$ ($\times 10^{-6}$) | normalized to $\int (I_{3'-6MAP*/T-T})$ d$\lambda$ | 5′-6MAP* $\lambda_{max}$ | $\int I_{5'-6MAP*}$ d$\lambda$ ($\times 10^{-6}$) | normalized to $\int (I_{5'-6MAP*/T-T})$ d$\lambda$ |
|---|---|---|---|---|---|---|
| probe | 428 | 147 (5) | 17.8 | 424 | 22.0 (1.2) | 4.2 |
| probe/T-T | 422 | 8.2 (1.0) | 1.0 | 418 | 5.3 (0.3) | 1.0 |
| probe/T<>T | 426 | 25.5 (2.4) | 3.1 | 422 | 9.4 (1.6) | 1.8 |
| probe/$PL_{ox}$ | 428 | 147 (2) | 17.5 | 426 | 23.5 (0.2) | 4.5 |
| probe/T-T/$PL_{ox}$ | 424 | 8.4 (0.3) | 1.0 | 418 | 5.7 (1.0) | 1.1 |
| probe/T<>T/$PL_{ox}$ | 428 | 46.6 (2.3) | 5.7 | 420 | 16.1 (0.8) | 3.1 |

least three separate experiments and preparations. A quantitative analysis is given in Table 3.

**5′-6MAP Emission Spectra.** The integrated fluorescence emission of the 5′-6MAP oligo was quenched by a factor of about 4.3 upon annealing to its complementary sequence (5′-6MAP/T-T). Addition of $PL_{ox}$ produced no further quenching of 5′-6MAP. The $\lambda_{max}$ for 5′-6MAP was 424 nm, compared to 418 nm for the duplex, suggesting that the 6MAP fluorophore experiences a more hydrophobic environment in duplex form, consistent with improved base stacking and reduced emission relative to its single-stranded state. Virtually no change in spectral shift was observed in either case when $PL_{ox}$ was included. The fluorescence intensities of the 5′-6MAP/$PL_{ox}$ and 5′-6MAP/T-T/$PL_{ox}$ systems showed almost no difference compared with their respective 5′-6MAP and 5′-6MAP/T-T samples, indicating that $PL_{ox}$ interacts weakly, if all, with the 6MAP probe in nonsubstrate ss- and ds-DNA.

Replacement of the T-T oligo with the T<>T strand led to large changes in emission intensities. The 5′-6MAP/T<>T emission increased by a factor of 1.8 relative to the 5′-6MAP/T-T duplex and was accompanied by a 4 nm red shift. This spectral shift and increase in emission is suggestive of base stacking disruption around the 6MAP probe, induced by the CPD. The integrated intensity of 5′-6MAP/T<>T/$PL_{ox}$ increased by a factor of 3.1 compared to 5′-6MAP/T-T and about 1.7 compared with 5′-6MAP/T<>T. The spectral shift was similar to that found for the damaged duplex without $PL_{ox}$.

**3′-6MAP Emission Spectra.** The emission quantum yield of 3′-6MAP was a factor of 6.7 higher than that of 5′-6MAP. This emission was unchanged in the presence of $PL_{ox}$. Surprisingly, the integrated fluorescence of the 3′-6MAP/T-T duplex was quenched by a factor of ~18 relative to 3′-6MAP, and was about 1.5 times higher in absolute intensity than that of the 5′-6MAP/T-T system. This is about 4−5 times the loss of intensity for the comparable 5′-6MAP system. As before, addition of $PL_{ox}$ left the emission unchanged. The $\lambda_{max}$ in 3′-6MAP emission was found at 428 nm, about 4 nm longer than that for the 5′ system. A 6 nm blue shift was observed in going from 3′-6MAP to 3′-6MAP/T-T.

The fluorescence intensity of the 3′-6MAP oligo was also highly quenched by the CPD-containing sequence, but the relative quench was about a factor of 2.7 less than the that for the 5′ system. The $\lambda_{max}$ shifted toward its single-stranded value, as was observed for the 5′ case. The fluorescence intensity of 3′-6MAP/T<>T/$PL_{ox}$ increased by a factor of ~2 compared to that of 3′-6MAP/T<>T, but was a factor of ~6 greater than that of the 3′-6MAP/T-T/$PL_{ox}$ duplex. This difference was ascribed to base flipping of the substrate into the protein accompanied by local disruption of base stacking in the probe on the complementary strand. The $\lambda_{max}$ of the 3′-6MAP/T<>T/$PL_{ox}$ emission was identical with that obtained for 3′-6MAP.

**Repair Assay Results.** 6MAP-containing duplexes were shown to be substrates of photolyase by performing repair assays. The repair assay was performed by monitoring 6MAP

fluorescence in CPD-containing duplexes in the presence of reduced photolyase under anoxic conditions while irradiating the protein with 365 nm light from the excitation monochromator of the fluorimeter. Repair is indicated by a decrease in 6MAP fluorescence as the repaired duplex is released with increased base stacking leading to better quenching of the probe. This change in fluorescence was normalized to the intensity after complete repair, and the averaged results for both duplexes from two separate trials are shown in Figure 6. Repair was evident in both cases, and there was no measurable difference in the rate of repair as a function of the position of the probe. This indicates that both 3′-6MAP/CPD and 5′-6MAP/CPD duplexes are true substrates of photolyase.

**6MAP Transition Dipole Moment.** To our knowledge, no data are available on the direction or magnitude of the transition dipole moment for the lowest energy optical transition of 6MAP. We employed time-dependent density functional theory to estimate this quantity, and the result of this calculation is shown in Scheme 1. The direction of the transition dipole moment in the molecular frame is represented as a double-headed arrow. The $y$-axis runs approximately parallel with the line passing through $N_3$ and $C_7$. The components of the transition dipole are $m_x = 0.56$ D, $m_y = -3.58$ D, and $m_z = -0.005$ D. The transition dipole direction was within 6° of the long axis of the molecule, with a negligible out-of-plane component of less than 0.2% of the total dipole magnitude. This is in contrast with the (experimentally determined) transition dipole moment for 2Ap,[43] which is tilted about 35° from the 2Ap long axis. This difference becomes important when considering energy transfer between either probe and the flavin cofactor (see below).

The magnitude of the transition dipole moment was calculated to be about 3.62 D. The gas-phase transition energy was 32 020 cm$^{-1}$ (312 nm). This value is about 18 nm blue-shifted from the absorption maximum in aqueous solution, $\lambda_{max} = 330$ nm. This result is expected in the case where the excited-state
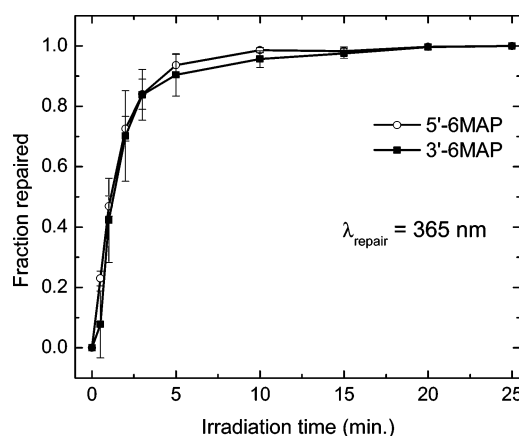


**Figure 6.** Normalized rates of repair for CPD-containing duplexes with 3′-6MAP(■) or 5′-6MAP (○) probes on the complementary strands.

**TABLE 4: Orientation Factors and FRET Parameters between Probes and FAD$_{ox}$**

| donor | 3′-2Ap* | 5′-2Ap* | 3′-6MAP* | 5′-6MAP* |
|---|---|---|---|---|
| $\kappa^2$ | 0.1 | 0.06 | 0.98 | 0.96 |
| $J$ (M$^{-1}$ cm$^{-1}$ nm$^4$) | $2.12 \times 10^{14}$ | $2.07 \times 10^{14}$ | $3.19 \times 10^{14}$ | $3.14 \times 10^{14}$ |
| $r_{DA}$ (Å) | 23.7 | 24.3 | 23.7 | 24.3 |
| $R_0$ (Å) | 19.8 | 14.9 | 28.7 | 21.0 |
| $\phi_{ET}$ | 0.25 | 0.05 | 0.76 | 0.29 |

permanent dipole moment is larger than the ground-state dipole moment, as is usually the case.

**Förster Resonance Energy Transfer (FRET).** The 6MAP emission spectrum overlaps well with the absorption spectrum of PL$_{ox}$, as shown in Figure 4a. This is true to a lesser extent for the 2Ap probe. It was natural to consider whether Förster resonance energy transfer[44] takes place in the 6MAP/T<>T/PL$_{ox}$ or the 2Ap/T<>T/PL$_{ox}$ complexes. This possibility was explored using the recent PL/CPD crystal structure,[17] which provided a "scaffold" onto which either 6MAP or 2Ap could be grafted and a calculation of the FRET efficiency performed. The efficiency for this process depends not only on donor–acceptor distance ($r_{DA}$) but also on the relative orientations of the probe transition dipole moments with the transition dipole moment of the oxidized FAD. In addition, spectral overlap is critical. The emission spectrum of 6MAP overlaps quite well with the S$_0$ → S$_1$ transition in the absorption spectrum of PL$_{ox}$. In contrast, 2Ap emission, which peaks at ca. 370 nm, overlaps the FAD S$_0$ → S$_2$ transition (spectrum not shown).

FRET efficiency depends on donor–acceptor distance as well as spectral overlap. The distance between the adenine bases complementary to the CPD and the FAD is about 24 Å, well within the range of FRET. This distance, $r_{DA}$, was obtained by calculating the center-to-center separation between the target purine (3′ or 5′) and the isoalloxazine, and is tabulated in Table 4 and Table S.1 (see Supporting Information).

The orientation factor $\kappa^2$ (eq 7) was calculated by replacing the 5′ or 3′ target adenine opposing the CPD with 6MAP or 2Ap. It was assumed that the analogue in the DNA kept the same orientation as that of the corresponding adenine and that the structure of oxidized FAD was identical to the reduced FAD in the PDB file. An example of the relative orientation of probe to the FAD is given in Figure 7. The flavin transition dipole moments, $\bar{m}_1$ and $\bar{m}_2$ for the S$_0$ → S$_1$ (450 nm) and S$_0$ → S$_2$ (370 nm) transitions respectively were obtained from linear dichroism spectra on single crystals of oxidized flavodoxin as measured by Eaton et al.[45]

Inspection of Table 4 shows that $\kappa^2$ was largest for the 3′-6MAP/FAD$_{ox}$ pair, followed by the 5′-6MAP/FAD$_{ox}$ couple. The $\kappa^2$ for the 3′-2Ap/FAD$_{ox}$ system was less than that for either of the 6MAP systems, and the smallest $\kappa^2$ was obtained for the 5′-2Ap/FAD$_{ox}$ pair. This trend is a direct consequence of the directions of the transition dipole moments of the probes and the fact that the 2Ap and 6MAP couple into different transition dipole moments of the flavin, which themselves have different directions in the molecular frame. It should be pointed out that no attempt was made to combine contributions from the two flavin transition dipole moments, even though emissions from the probes have some spectral overlap with both transitions. This can be seen qualitatively by close examination of the PL$_{ox}$ absorption spectrum in Figure 4a, showing the 6MAP emission overlaps best with the 450 nm transition of FAD$_{ox}$ while the 370 nm transition of the flavin would overlap well with 2Ap emission centered at 370 nm. The overlap integrals calculated in this study range from $2 \times 10^{14}$ to ∼$3 \times 10^{14}$ M$^{-1}$ cm$^{-1}$ nm$^4$, similar to that obtained for the folate-to-FADH$^-$ donor–acceptor couple studied by Kim et al.[12]

FRET efficiencies also depend on the quantum yield of the donor, $\phi_D$ (see Supporting Information). The quantum yields of the 3′-6MAP and 5′-6MAP oligos were estimated by using the fluorescence quantum yield of 6MAP monomer, 0.39,[24] and the ratio of the fluorescence intensity of 6MAP monomer to that of 3′-6MAP or 5′-6MAP at the same concentration (data not shown). 6MAP monomer fluorescence intensity was linear over the range of concentrations studied, indicating that quenching due to dimerization was negligible (data not shown).

The calculated $R_0$ values were used to directly calculate the FRET efficiencies (eq 6). $\phi_{ET}$ (eq 5) was largest for the 6MAP complexes and decreased significantly for the 2Ap complexes, a direct result of the orientation of transition dipole moments ($\kappa^2$) for these complexes. In particular, the 3′-6MAP/T<>T/PL$_{ox}$ system has a calculated FRET efficiency of $\phi_{ET} = 0.76$. The 5′-6MAP system is significantly less efficient: $\phi_{ET} = 0.29$. The 2Ap systems show lower FRET values, with $\phi_{ET} = 0.25$ and $\phi_{ET} = 0.05$ for the 3′ and 5′ systems, respectively.

$\kappa^2$ was calculated assuming that the probe occupies the same orientation in the protein:substrate complex as the native adenine it replaces. We have chosen the short axis of the adenine bases as a reference angle, $\theta_{xtal}$, against which the transition dipole moment is defined relative to the crystal structure. However, it may be the case that both the 2Ap and the 6MAP will have
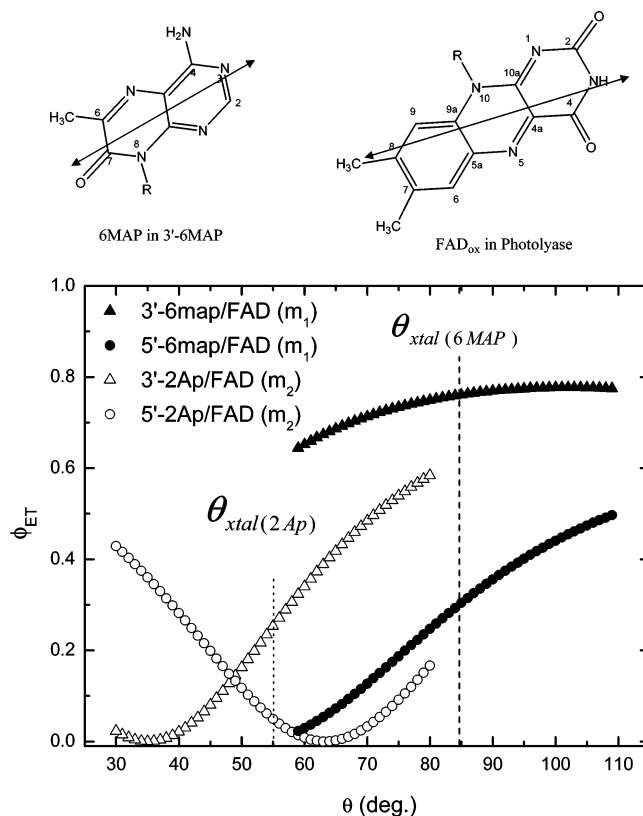


6MAP in 3′-6MAP        FAD$_{ox}$ in Photolyase



**Figure 7.** Orientations of 6MAP and FAD$_{ox}$ modeled on the Mees et al. crystal structure[17] and the sensitivity of the % FRET efficiency on the transition dipole moment angle relative to the short axis of the probe molecule. The dashed lines refer to the angles used in the FRET calculation.

6MAP, a Probe of Base Flipping by DNA Photolyase

*J. Phys. Chem. B, Vol. 111, No. 35, 2007* **10623**

different orientations than we have assumed. The sensitivity of $\phi_{ET}$ against the transition dipole moment angle relative to the short axis of the probe was calculated, and the results are plotted in Figure 7. The broken lines indicate the angle $\theta_{xtal}$ between the short axis of the probe and its transition dipole moment. Deviations from $\theta_{xtal}$ translate into conformations that differ from the assumed conformation. While the exact $\theta$ remains unknown, the prediction that the 6MAP probe has much higher FRET efficiency than 2Ap should be true for any physically reasonable $\theta$.

If FRET is occurring, then a diminution of 430 nm 6MAP emission should be accompanied by an increase in 520 nm FAD emission. Contrary to our calculations, no increase in FAD emission was observed at 520 nm for any of the systems studied, beyond that observed because of the direct excitation of the cofactor itself. The rationale for this observation, FAD quenching in the protein, is explored below.

## Discussion

**Absorption Measurements.** The largest blue shift in the absorption of the 6MAP probe occurred for the 3′-6MAP/T-T duplex. This would suggest that the fluorophore is in a more hydrophobic environment than the 5′-6MAP/T-T system. Similar shifts for 2-Ap have been reported previously,[41] but to our knowledge there are few data on this effect for 6MAP.

**Thermostability of Probe- and Lesion-Containing Double Helices.** The replacement of adenine by 6MAP led to a decrease of the $T_m$. A plausible explanation for this change is the bulky methyl group on the pteridone, which may produce less favorable base stacking in the duplex. This interpretation would be consistent with the smaller quench observed upon duplex formation for 6MAP vs 2Ap, if the quenching effect of the 3′-purine on 2Ap is taken into account.

From the melting temperature experiments, the CPD lowers the local and global melting points significantly (~6−10 °C) relative to the non-CPD duplex. This is also seen by comparing the fluorescence intensity of the CPD-containing duplex with that of the T-T duplex. The fluorescence intensity of CPD-containing duplex is more than that of the perfectly matched duplex, which indicates that the CPD destabilizes base stacking locally. Experiments are in progress to determine the extent of base stacking disruption. This result is also consistent with a recent crystal structure of a CPD-containing dodecamer in which the CPD is somewhat destacked with slightly elongated Watson−Crick hydrogen bonds.[46] Similarly, the melting point depression is similar to what one would expect from the introduction of an abasic site into the duplex. However, previous enthalpy determinations for the introduction of a CPD into short DNA duplexes show little difference between the enthalpy with and without the CPD[46] determined under similar conditions and by similar methods. The reason for this discrepancy is not yet understood.

Consistent with the $T_m$ measured by the fluorescence method, there is about a 10 °C difference between the melting points of CPD-containing duplex and T-T-containing duplex. Comparing the melting temperatures of 6MAP-containing duplexes measured by fluorescence and absorbance methods, $T_m$ values measured by the absorbance method are higher than those measured by fluorescence. This indicates that local melting happens earlier than global melting and that the transition cannot be well described as a two-state process.

Taken at face value, the 3′-6MAP probe destabilizes both the undamaged and CPD-containing duplexes by nearly −20 kcal/mol compared to −10 kcal/mol for the 5′-6MAP system.

The $T_m$ values corroborate this observation, although the relative difference is less. This effect could be due to sequence-specific quenching of the probe based on its 5′ and 3′ neighbors. Such behavior has been documented for 2-aminopurine, but propensity rules for 6MAP are not as clear-cut.[25] This interpretation is further supported by examining the differences in free energy based on a Watson−Crick base pair nearest-neighbor analysis for the native bases. The 5′-6MAP probe is bracketed by 5′-CC<u>P</u>AC-3′ compared to 5′-CA<u>P</u>CT-3′ for the 3′-6MAP construct. Using tabulated values of nearest-neighbor free energies[47] surrounding the central <u>P</u>/T (A/T) region, it is estimated that the 5′-6MAP oligo (5′-CC<u>P</u>AC-3′) has $\Delta G° = -5.77$ kcal/mol compared to $\Delta G° = -5.17$ kcal/mol for the 3′-6MAP oligo (5′-CA<u>P</u>CT-3′) at 37 °C. This suggests that the degree of single-stranded base stacking in the 5′-6MAP oligo is significantly greater than that in the corresponding 3′-6MAP oligo. Thus, at low temperature the 5′-6MAP fluorescence would be quenched compared to 3′-6MAP, but this difference would disappear upon annealing to the complementary strand.

**Emission Spectra of the Duplexes.** The emission maximum of the 3′-6MAP probe is consistently red-shifted relative to the 5′-6MAP probe, which is similar to the results obtained for A-tracts in 6MAP-containing duplexes.[42] The shift is obtained even for ss-DNA as well as the complementary duplexes (e.g., 3′-6MAP/T-T). This suggests that the 6MAP probe in the 3′ position is more solvent exposed than that in the 5′ position, which is consistent with a loss of base stacking, hence quenching, in the 3′ system. This is the case for probe-containing single-stranded DNA and for the base-flipped substrate:protein complexes where the 3′-6MAP integrated intensity is about 2−6 times larger than that for the corresponding 5′-6MAP species. However, when duplexes are formed with the complementary (T-T) strand, this difference in intensity is much smaller, indicating that there is little perturbation in the double helical structure induced by the 6MAP molecule.

This is not true for CPD-containing DNA. The source of this differential emission, however, is unclear. It may be that the CPD reduces the degree of base stacking at the 3′ site of the probe-containing strand. Alternatively, this effect may be true for this sequence only. The probe in the 5′-6MAP strand is bracketed by C<u>P</u>A, while the 3′-6MAP probe is bracketed by A<u>P</u>C. It is also possible that the intensity changes are due to a combination of these factors. As stated above, quenching rules in 6MAP are poorly understood and further experimentation is necessary to understand the source of the differential emission.

The largest red shift is obtained for 3′-6MAP/CPD/PL$_{ox}$, about −8 nm. This observation is in agreement with our previous work using 2Ap,[5,19] and suggests that 6MAP is the most solvent exposed in this substrate:protein complex, which is also consistent with previous studies.[17,20,48] The lower relative emission for the 3′-6MAP base-flipped substrate compared to the 5′-6MAP base-flipped substrate is not found in the corresponding 2Ap substrates.[5,19] The reason for this disagreement is explored below.

**Sequence Dependence of the Fluorescence Quantum Yield and FRET.** The fluorescence intensity of the single-stranded 3′-probe oligo is higher than that of 5′-probe oligo. This suggests that the 3′-6MAP oligo is less base stacked in single-stranded form than the 5′-6MAP oligo. This intensity pattern is also the rule for all duplexes. The observed differences could be due in part to differences in orbital overlap of the pteridone with neighboring bases. The differential orbital overlap could be due to the electronic structure of 6MAP, or to structural differences in the duplex (e.g., steric clashes caused by the methyl group

in 6MAP). Our data provide no direct way of distinguishing between these two cases. However, it is clear that the fluorescence quantum yield of 6MAP is sensitive to base stacking and this makes it a valuable tool for studying base flipping.

A comparison of the base-flipping results for the two probes shows that the 2Ap system is about 1.5−2 times more emissive, compared to its unflipped state, than 6MAP in providing a base-flipping signal. However, this result must be considered in the context of energy transfer between the probe and the FAD cofactor. Our FRET calculations show that 6MAP in the 3′ position should transfer energy with high efficiency to FAD$_{ox}$. In fact, 3′-6MAP should lose about 76% of its excitation energy to FRET compared to 25% for 3′-2Ap. A comparison of the integrated signal intensities for 3′-6MAP/T<>T/PL$_{ox}$ to 3′-2Ap/T<>T/PL$_{ox}$[19] does not give this large a difference. One possibility is that our FRET calculations are too approximate to be of predictive value. However, fluorescence quenching from other sources, such as charge transfer or loss of oscillator strength, cannot be neglected. These alternate pathways could effectively compete with FRET to give the observed ratios.

As mentioned earlier, the absorbance peaks of the oxidized FAD inside DNA photolyase overlap the emission peaks of 2Ap (about 370 nm) and 6MAP (about 430 nm). In the complex of oxidized DNA photolyase and probe containing substrate duplex, the distance between the probe and FAD is around 24 Å, which is within the Förster resonance energy transfer range. Interestingly, this value, along with the overlap integral, is similar to what was found for the energy transfer step between the folate light-harvesting antenna and the semiquinone FADH• in native photolyase.[12] In this case, the donor−acceptor distance was about 32 Å and the overlap integral was $2 \times 10^{14}$ cm$^3$ M$^{-1}$.

Based on the experiments we have done so far, no obvious fluorescence intensity increase of oxidized FAD in photolyase has been observed. There are several possible reasons for this. One is that FRET is taking place from the adenine analogue to FAD; however, after energy transfer to FAD, $^1$FAD does not emit because of its low fluorescence quantum yield. Oxidized flavin mononucleotide (FMN) is highly fluorescent. Its fluorescence quantum yield is about 0.26.[49,50] However, the fluorescence of oxidized FAD is much weaker than that of oxidized FMN because FAD fluorescence is quenched by stacking with its adenine moiety. The fluorescence quantum yield of oxidized FAD in aqueous solutions at neutral pH is reduced to only 1/10 that of oxidized FMN.[51] Moreover, the fluorescence intensity of oxidized FAD in photolyase was 8-fold less than that of free oxidized FAD.[52] Therefore, the fluorescence quantum yield of oxidized FAD in photolyase is about 0.002.

If we assume that base flipping in the absence of FRET gives $1.8 \times 10^6$ counts (the peak signal for the 3′-6MAP ss-DNA oligo), then the signal after FRET would be around 2700 counts at 520 nm, the peak of PL$_{ox}$ emission. This is close to the Poisson error expected in the FRET process (about 1300 counts). The maximum signal obtained in the 3′-6MAP/T<>T/PL$_{ox}$ experiment at 520 nm was about $3.4 \times 10^4$ counts. Most of this light is from the red edge of the 6MAP emission spectrum, which overlaps the FAD emission. It is therefore not surprising that FAD fluorescence is difficult to observe even with high-efficiency FRET from the 6MAP fluorophore. It will be necessary to measure the emission from both chromophores on the picosecond time scale to ascertain whether FRET is operative in this system.

**Structural Considerations.** A consideration of the recent protein:product analogue crystal structure from Mees et al.[17] is important in understanding the solution-state results we have obtained using the fluorescent probe approach. This crystal structure was obtained with a modified double-stranded substrate where the phosphate group was replaced with a formacetal linkage to confer greater stability to hydrolysis. The crystal structure revealed that the CPD had been repaired, apparently from photoelectrons produced in the crystal by the X-ray source. However, the repaired thymidines are shown inside the substrate-binding pocket of the protein, so it is reasonable to assume that this configuration is close to the in vivo structure prior to repair. The complementary strand of the duplex shows that the 3′-A is slightly less base stacked than the 5′-A. However, the difference is small and it would be difficult to rationalize the increased emission from either 2-Ap or 6-MAP on this basis alone.

It is important to highlight that our work was done on the *E. coli* photolyase:CPD complex. However, the analysis of the *Anacystis nidulans* structure showed that almost no change occurs to the binding site upon binding the lesion.[17] In addition, the residues in the binding site are highly conserved. To make the comparison, we choose the NH$_2$ group of the FAD adenine as a reference point for both structures, as it is within van der Waals contact of the CPD based on the *A. nidulans* structure. The residues within about 6 Å of the NH$_2$-Ado in *A. nidulans* are Glu283, Trp286, Arg287, Tyr290, and Asn349. These residues interact strongly with the CPD. The same set of residues are found in the *E. coli* protein (Glu274, Trp277, Arg278, Tyr281, and Asn341) which are within 6 Å in the NH$_2$-Ado of that structure as well. Based on the lack of a conformational change upon substrate binding and the high sequence homology, we think that the energy transfer parameters obtained from this hybrid approach are reasonable.

The repair assay demonstrates that the placement of the 6MAP probe in either position relative to the CPD does not alter the relative rate of repair. These results are consistent with similar experiments performed on 5′-2Ap-containing duplexes from our previous study. Of course, these measurements do not prove that the kinetics of electron transfer or bond breaking in the complex are the same as for native DNA. All that can be said at this point is that 6MAP does not appear to alter the way in which the protein recognizes its substrate ($k_{on}$) or releases its product ($k_{off}$). This suggests that 6MAP is an excellent and versatile probe of CPD repair in other systems.

## Conclusions

6MAP is a fluorescent adenine analogue that demonstrates high sensitivity to base-stacking interactions in duplex DNA. It is capable of reporting changes in local helical structure due to CPD base flipping in the presence of DNA photolyase and does not appear to alter substrate recognition substantively. The transition dipole moment of the lowest energy optical band was computed using TDDFT, showing that this vector lies nearly along the long axis of the molecule. Based on emission yield data, the 3′ position of the complementary strand opposing the CPD lesion appears be significantly less stacked than the 5′ position, but its fluorescence quantum yield is much lower than expected, perhaps due to FRET. The apparently greater sensitivity of the 2-Ap analogue to base flipping may be due to a reduced FRET efficiency compared to the 6MAP analogue.

**Abbreviations.** CPD, cyclobutylpyrimidine dimer; 2Ap, 2-aminopurine; 6MAP or P, 4-amino-6-methyl-8-(2′-deoxy-β-D-ribofuranosyl)-7(8H)-pteridone; ss, single-stranded; ds, double-stranded; PL$_{ox}$, oxidized DNA photolyase; 5′-2Ap, 5′-CTCC-2Ap-ACTTGC-3′; 3′-2Ap, 5′-CTCCA-2Ap-CTTGC-3′; FAD, flavin adenine dinucleotide; FAD$_{ox}$, oxidized FAD; FADH$^-$, reduced anionic FAD hydroquinone; FMN, flavin mononucle-

6MAP, a Probe of Base Flipping by DNA Photolyase

*J. Phys. Chem. B, Vol. 111, No. 35, 2007* **10625**

**Supporting Information Available:** Supplementary data for FRET calculations. This material is available free of charge via the Internet at http://pubs.acs.org.

## References and Notes

(1) Roberts, R. J. *Cell* **1995**, *82* (1), 9.

(2) Stivers, J. T.; Pankiewicz, K. W.; Watanabe, K. A. *Biochemistry* **1999**, *38*, 952.

(3) McCullough, A. K.; Dodson, M. L.; Scharer, O. D.; Lloyd, R. S. *J. Biol. Chem.* **1997**, *272*, 27210.

(4) Butenandt, J.; Burgdorf, L. T.; Carell, T. *Angew. Chem., Int. Ed.* **1999**, *38*, 708.

(5) Christine, K. S.; MacFarlane, A. W., IV; Yang, K.; Stanley, R. J. *J. Biol. Chem.* **2002**, *277*, 38339.

(6) Holz, B.; Klimasauskas, S.; Serva, S.; Weinhold, E. *Nucleic Acids Res.* **1998**, *26*, 1076.

(7) Allan, B. W.; Beechem, J. M.; Lindstrom, W. M.; Reich, N. O. *J. Biol. Chem.* **1998**, *273*, 2368.

(8) Allan, B. W.; Reich, N. O. *Biochemistry* **1996**, *35*, 14757.

(9) Sancar, A. *Chem. Rev.* **2003**, *103*, 2203.

(10) Langenbacher, T.; Zhao, X.; Bieser, G.; Heelis, P. F.; Sancar, A.; Michel-Beyerle, M. E. *J. Am. Chem. Soc.* **1997**, *119*, 10532.

(11) Kim, S. T.; Heelis, P. F.; Sancar, A. *Biochemistry* **1992**, *31*, 11244.

(12) Kim, S. T.; Heelis, P. F.; Okamura, T.; Hirata, Y.; Mataga, N.; Sancar, A. *Biochemistry* **1991**, *30*, 11262.

(13) Heelis, P. F.; Okamura, T.; Sancar, A. *Biochemistry* **1990**, *29*, 5694.

(14) MacFarlane, A. W., IV; Stanley, R. J. *Biochemistry* **2003**, *42*, 8558.

(15) Kao, Y.-T.; Saxena, C.; Wang, L.; Sancar, A.; Zhong, D. *Proc. Natl. Acad. Sci. U.S.A.* **2005**, *102*, 16128.

(16) Park, H.-W.; Kim, S.-T.; Sancar, A.; Deisenhofer, J. *Science* **1995**, *268*, 1866.

(17) Mees, A.; Klar, T.; Gnau, P.; Hennecke, U.; Eker, A. P. M.; Carell, T.; Essen, L.-O. *Science (Washington, DC, U.S.)* **2004**, *306*, 1789.

(18) Torizawa, T.; Ueda, T.; Kuramitsu, S.; Hitomi, K.; Todo, T.; Iwai, S.; Morikawa, K.; Shimada, I. *J. Biol. Chem.* **2004**, *279*, 32950.

(19) Yang, K.; Stanley, R. J. *Biochemistry* **2006**, in press.

(20) Berg, B. J. V.; Sancar, G. B. *J. Biol. Chem.* **1998**, *273*, 20276.

(21) Jorns, M. S.; Baldwin, E. T.; Sancar, G. B.; Sancar, A. *J. Biol. Chem.* **1987**, *262*, 486.

(22) Ward, D. C.; Reich, E.; Stryer, L. *J. Biol. Chem.* **1969**, *244*, 1228.

(23) Nordlund, T. M.; Andersson, S.; Nilsson, L.; Rigler, R.; Graeslund, A.; McLaughlin, L. W. *Biochemistry* **1989**, *28*, 9095.

(24) Hawkins, M. E.; Pfleiderer, W.; Jungmann, O.; Balis, F. M. *Anal. Biochem.* **2001**, *298*, 231.

(25) Hawkins, M. E.; Pfleiderer, W.; Balis, F. M.; Porter, D.; Knutson, J. R. *Anal. Biochem.* **1997**, *244*, 86.

(26) Stanley, R. J.; MacFarlane, A. W., IV. *J. Phys. Chem. A* **2000**, *104*, 6899.

(27) Heelis, P. F.; Payne, G.; Sancar, A. *Biochemistry* **1987**, *26*, 4634.

(28) MacFarlane, A. W., IV; Stanley, R. J. *Biochemistry* **2001**, *40*, 15203.

(29) Wang, B.; Jorns, M. S. *Biochemistry* **1989**, *28*, 1148.

(30) Payne, G.; Wills, M.; Walsh, C.; Sancar, A. *Biochemistry* **1990**, *29*, 5706.

(31) Banerjee, S. K.; Christensen, R. B.; Lawrence, C. W.; LeClerc, J. E. *Proc. Natl. Acad. Sci. U.S.A.* **1988**, *85*, 8141.

(32) Petersheim, M.; Turner, D. H. *Biochemistry* **1983**, *22*, 256.

(33) Santalucia, J., Jr. *Spectrophotometry and Spectrofluorimetry*, 2nd ed.; 2000; p 329.

(34) Mikulecky, P. J.; Feig, A. L. *Biochemistry* **2006**, *45*, 604.

(35) Press, W. H.; Flannery, B. P.; Teukolsky, S. A.; Vetterling, W. T. *Numerical Recipes in C The Art of Scientific Computing*; Cambridge University Press: New York, 1988.

(36) Becke, A. D. *J. Chem. Phys.* **1993**, *98*, 5648.

(37) Krishnan, R.; Binkley, J. S.; Seeger, R.; Pople, J. A. *J. Chem. Phys.* **1980**, *72*, 650.

(38) Aprà, E.; Windus, T. L.; Straatsma, T. P.; Bylaska, E. J.; de Jong, W.; Hirata, S.; Valiev, M.; Hackler, M.; Pollack, L.; Kowalski, K.; Harrison, R.; Dupuis, M.; Smith, D. M. A; Nieplocha, J.; Tipparaju, V.; Krishnan, M.; Auer, A. A.; Brown, E.; Cisneros, G.; Fann, G.; Früchtl, H.; Garza, J.; Hirao, K.; Kendall, R.; Nichols, J.; Tsemekhman, K.; Wolinski, K.; Anchell, J.; Bernholdt, D.; Borowski, P.; Clark, T.; Clerc, D.; Dachsel, H.; Deegan, M.; Dyall, K.; Elwood, D.; Glendening, E.; Gutowski, M.; Hess, A.; Jaffe, J.; Johnson, B.; Ju, J.; Kobayashi, R.; Kutteh, R.; Lin, Z.; Littlefield, R.; Long, X.; Meng, B.; Nakajima, T.; Niu, S.; Rosing, M.; Sandrone, G.; Stave, M.; Taylor, H.; Thomas, G.; van Lenthe, J.; Wong, A.; Zhang, Z. *NWChem, A Computational Chemistry Package for Parallel Computers*, version 4.7; Pacific Northwest National Laboratory: Richland, WA, 2005.

(39) Bloomfield, V. A.; Crothers, D. M.; Tinoco, I. J. *Physical chemistry of nucleic acids*; Harper and Row: New York, 1974.

(40) Park, H.; Zhang, K.; Ren, Y.; Nadji, S.; Sinha, N.; Taylor, J.-S.; Kang, C. *Proc. Natl. Acad. Sci. U.S.A.* **2002**, *99*, 15965.

(41) Law, S. M.; Eritja, R.; Goodman, M. F.; Breslauer, K. J. *Biochemistry* **1996**, *35*, 12329.

(42) Augustyn, K. E.; Wojtuszewski, K.; Hawkins, M. E.; Knutson, J. R.; Mukerji, I. *Biochemistry* **2006**, *45*, 5039.

(43) Holmen, A.; Norden, B.; Albinsson, B. *J. Am. Chem. Soc.* **1997**, *119*, 3114.

(44) Cantor, C. R.; Schimmel, P. R. *Biophysical Chemistry*; W. H. Freeman and Co.: New York, 1980; Vol. 2.

(45) Eaton, W. A.; Hofrichter, J.; Makinen, M. W.; Andersen, R. D.; Ludwig, M. L. *Biochemistry* **1975**, *14*, 2146.

(46) Jing, Y.; Kao, J. F. L.; Taylor, J.-S. *Nucleic Acids Res.* **1998**, *26*, 3845.

(47) SantaLucia, J., Jr.; Hicks, D. *Annu. Rev. Biophys. Biomol. Struct.* **2004**, *33*, 415.

(48) Husain, I.; Sancar, G. B.; Holbrook, S. R.; Sancar, A. *J. Biol. Chem.* **1987**, *262*, 13188.

(49) Weber, G. *Biochem. J.* **1950**, *47*, 114.

(50) Kotaki, A.; Naoi, M.; Yagi, K. *J. Biochem.* **1970**, *68* (3), 287.

(51) Barrio, J. R.; Tolman, G. L.; Leonard, N. J.; Spencer, R. D.; Weber, G. *Proc. Natl. Acad. Sci. U.S.A.* **1973**, *70*, 941.

(52) Jorns, M. S.; Wang, B.; Jordan, S. P.; Chanderkar, L. P. *Biochemistry* **1990**, *29*, 552.